

PERFORMANCE ANALYSIS OF A TWO NODE RADAR NETWORK GEOMETRY ON ORBIT ESTIMATION ACCURACY

Cordula Knauf⁽¹⁾, Rudolf Hoffmann⁽¹⁾, Hans Schily⁽²⁾, Dr. Alexander Charlish⁽²⁾, Miriam Martin Gonzalez⁽³⁾, and Dr. Robert Kohlleppel⁽⁴⁾

⁽¹⁾Fraunhofer FHR, 53343 Wachtberg Germany, Email: firstname.surname@fhr.fraunhofer.de

⁽²⁾Fraunhofer FKIE, 53343 Wachtberg Germany, Email: firstname.surname@fkie.fraunhofer.de

⁽³⁾Fraunhofer FHR, 53343 Wachtberg Germany, present Email: miriam.mg@myriadgarden.com

⁽⁴⁾Fraunhofer FHR, 53343 Wachtberg Germany, present Email: robert@kohlleppel.net

ABSTRACT

Multistatic radar systems are emerging as an important tool for low earth orbit space surveillance. The improved coverage and multiple observation perspectives provided by multistatic systems lead to improved space debris detection and orbit estimation accuracy. This paper investigates the influence of different baselines between two radar nodes on the orbit estimation performance of space targets. We consider briefly the influence of the field of view and two different radar modes on the optimal baseline. For our results we use the Posterior Cramer-Rao Lower Bound, which generates a lower bound on the expected error from any tracking algorithm. Hence, our results are only comparable with each other. The presented framework can be used to design a multistatic radar network for given requirements on target detection and tracking capabilities.¹

Keywords: Radar, space debris, multistatic signal path, radar networks, node configuration, surveillance and tracking of low earth orbits, multistatic radar systems.

1. INTRODUCTION

Modern society heavily depends on satellites. To avoid a fatal collision between space debris and a functional satellite, the position of debris has to be predicted for any given point in time. Based on the prediction, an active satellite is able to perform evasive maneuvers.

Space debris is observed with many resources. For instance, observations are possible with optical methods [1] like laser ranging [2] or radar.

Traditionally, a single large monostatic radar is used for Space Surveillance. In [3] the benefits of multistatic radars, like improved coverage and multiple observation

perspectives, are explained for the generic case. Recent studies aim at applying the benefits of multiple radar systems to the observation of objects in space environment. Existing radar networks include EISCAT (European Incoherent Scatter Scientific Association), founded originally for better modeling of the atmosphere. Tests have revealed that the next generation of radars (EISCAT_3D) will also be capable of observing space debris [4]. Another example system is GRAVES (*Grand Réseau Adapté à la Veille Spatiale*), which is a bistatic radar especially designed for space surveillance [5]. The German state is developing a radar system called GESTRA (German Experimental Space Surveillance and Tracking Radar), which is designed to allow a more flexible positioning of sensor nodes due to semi-portable receivers and transmitters [6]. All of these systems provide important information to avoid a crash between space debris and a functional satellite.

To calculate the collision risk of space debris observations are required. The observations of this paper are based on phased array radar network. The radar observes an arbitrary object at n points in a given time interval t_n . These observations are used to derive parameters of a model, which leads to the position and the velocity of the object for any arbitrary future point i in time t_i . For the purpose of this paper it is sufficient to model space debris trajectories using simple Keplerian motion. This model does not consider perturbations like effects from the moon, sun or inhomogeneity of the mass distribution of the earth. Generally, six non-redundant parameters are necessary to describe a Kepler orbit without any additional perturbations. In this context, the parameter vector (6×1), also called state vector, consists of the position and the velocity of an object at a given point in time. Estimating these six parameters based on radar observations is crucial for planning evasive maneuvers. Unfortunately, noise corrupts the observations, leading to noisy parameters and inaccurate collision risk calculations.

Beside noise the estimation accuracy is also affected by the properties of the radars, like array size or dwell time,

¹The project underlying the presented results was funded by the German Federal Ministry of Education and Research under the code 50 LZ 1503. The author is responsible for the content of this publication.

signal processing methods and many more aspects. Due to the variety of variables, optimizing the performance of a radar network for orbit estimation accuracy is a highly complex task. This paper focuses on optimizing the baseline between two radars for best orbit estimation accuracy. Beside other factors, the optimal baseline is also dependent on the field of view (FoV) and radar modes. Hence, two different FoV's, a search mode and a track mode are taken into account. In Section 2 the general simulation setup is explained. The calculation of the state parameters and their accuracies is briefly presented in Section 3, together with the results of our simulations.

2. SIMULATION SETUP

The accuracy of parameter estimation is dependent on many factors. Each radar parameter influences the outcome. Furthermore, the constellation between a space debris object and the node configuration has an impact on the accuracy. Different constellations lead to different lengths of observation times and different aspect angles, which lead to different bistatic ranges. As a result the Signal to Noise Ratio (SNR) and the detection probability varies significantly for different constellations. To compensate the effect of different constellations, we simulate and observe multiple orbits for one month. The node configurations regarding varying baselines are analyzed with fixed radar parameters. To get a first insight on the influence of the field of view (FoV) and radar modes, three basics setups are considered during the analysis of an optimal baseline.

2.1. FoV Setup

The FoV describes the area in space, which is illuminated by a radar. Within this area, observations of a space object are possible. The extension of a FoV gets bigger for higher orbits, as depicted in Fig. 1. Therefore, an object is longer within the FoV if the object has a higher orbit. A longer observation time is possible as a result. The extent of the shown FoV is 15° in elevation and 90° in azimuth with respect to the transmitter (Tx). The whole FoV can

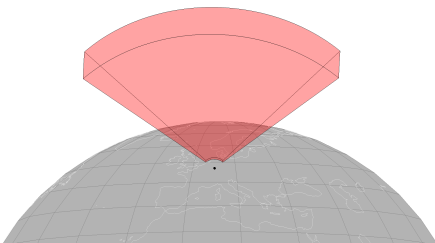


Figure 1: Horizontal FoV of a radar - extension elevation 15° , azimuth 90°

not be scanned by a single Tx beam at once, because the radar beamwidth is in our simulation 5° wide and not 15°

x 90° . To illuminate the whole FoV with just one beam in a given time interval different approaches are possible. In this paper, we focus on a track mode and a basic search mode. The track mode knows in our simulation exactly where an object is located. Hence, the transmitter only illuminates the spot where an object is predicted. That is why, the track mode generate observations whenever an object crosses the FoV. While the track mode requires information about an object, the search mode works perfectly without any object information. The FoV is searched by activating each beam position for a short period of time, before moving to the next beam position. Each beam position in this search is illustrated as a red cone in Fig. 2 and is active for the dwell time. After

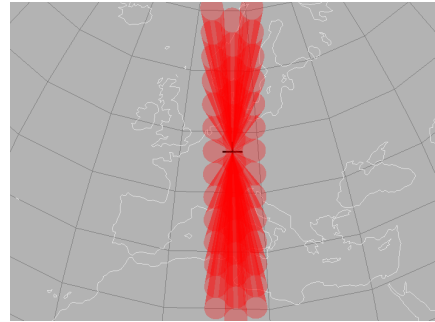


Figure 2: Search mode, vertical FoV - extension elevation 90° , azimuth 15°

this time, the next beam is activated. The extent of the shown FoV is 90° in elevation and 15° in azimuth with respect to the transmitter. A single radar node monitors the whole FoV. Observations are only simulated if the object is within the FoV and the timing of an active beam. An optimal baseline is dependent on the orientation of the FoV and the radar mode. To get a first understanding of the impact on these factors on finding the optimal baseline for orbit estimation accuracy, three different setups are used in this paper. Setup I is a search mode with a vertical FoV (see Fig. 2), setup II has a horizontal FoV and a search mode and setup III is the track mode shown in Fig 1. For later reference these setups are listed in Tab. 1

Table 1: List of setup parameters - each setup is tested with all simulated length of baselines

	Setup I	Setup II	Setup III
Radar mode	Search	Search	Track
FoV elevation	90°	15°	15°
FoV azimuth	15°	90°	90°

2.2. Radar Setup

A horizontal baseline is the basis for all node configurations under investigation. In Fig. 3 one configuration is

shown. One transmitter and receiver (Tx/Rx) is placed at the first node and one Rx is placed at the second node. Hence, in total, three sensors are available. Baselines between 50 to 950 km with steps of 50 km are tested. For baselines higher than 950 km the simulation parameters deliver an SNR below the detection threshold, such that multistatic measurements are not possible. The center of the network is placed in Germany.

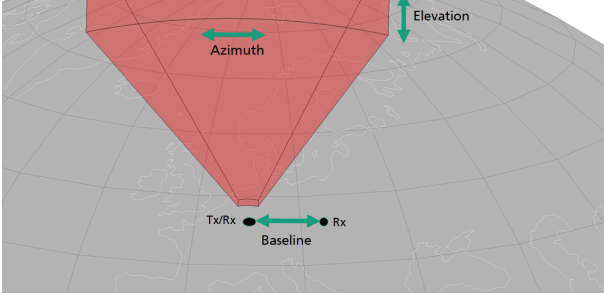


Figure 3: Tested configuration- center of network is in Germany

In Tab. 2 the specific radar parameters for this simulation are listed, which apply to all measurements.

Table 2: Specific fixed radar parameters for this simulation

average power	20000 Watt
dwelt time	0.2 s
effective aperture size	$3.5 m^2$
radar cross section (RCS)	$5 m^2$
wavelength	0.2 m
beamwidth	0.0886 rad
range resolution	132.8 m
angle resolution	0.0089 rad
bandwidth	1 MHz

2.3. Orbit Setup

Each orbit has a different ground track. These ground tracks vary due to earth's rotation. There are some orbits, called repeat orbits, with constant ground tracks, but these are not considered in this paper. To minimize the influence of different ground tracks, multiple orbits and multiple periods of these orbits are simulated within one month. In the context of this paper, simulated Kepler parameters are used instead of real objects. The orbit inclination is between 45° and 90° in steps of 5° and the orbit height is between 300 km and 1600 km in steps of 100 km. For higher orbits the observed SNR is below the threshold. Changing the radar parameter or using different signal processing technique could alleviate this. However, these topics are not discussed within this paper. Also, orbits with a smaller inclination than 45° are not considered. The limitation of the inclination is due to

the fact that the center of the nodes is placed in Germany. In total, 140 Kepler orbits, but without modeled perturbations, are taken into account. In Fig. 4 all considered orbits are visualized.

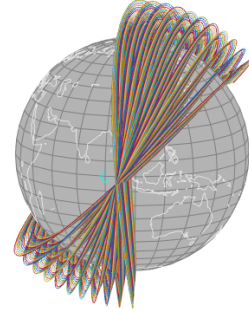


Figure 4: 140 orbits are simulated for state vector estimation

2.4. Simulated Observations for one Setup

For each of the 19 baseline configurations observations are simulated of all 140 orbits (see Fig. 4) for a duration of one month. If an observation is possible and the SNR is above a given detections threshold of 11 dB, an observation is generated. Each observation contains three measurements, namely range, azimuth angle and elevation angle. Doppler measurements are not considered here. The RCS is assumed to be constant. Based on these observations the position and velocity of a space object are estimated. We assume, that the association of observation to object is solved. In addition, it is assumed that the time synchronizations between different stations is perfect.

3. RESULTS

This section presents the simulation results by comparing the accuracies of the estimated state vectors. The evaluated metric is the Posterior Cramer-Rao Lower Bound, which presents the lower bound of the achievable accuracy. Furthermore, there are no errors due to non modeled perturbations. Consequently, the accuracies in this paper are much lower than practically achievable. However, the results can be used for a relative comparison between node configurations.

3.1. Estimation of State Vector plus Accuracies

Commonly in tracking tasks, Kalman Filters are used to obtain trajectories from measurements [7]. The Kalman filter relies on a prediction and measurement update step. We use Cowell's Formulation and a fourth order Runge-Kutta numerical integration scheme for predicting targets exerting Keplerian motion [8]. Fig. 5 visualizes the update scheme in use. For the initial detection no a priori information is available and the first two detections are used to generate a first estimate of the state vector. Else, prior information is available from previous passes and this information is used to improve the state vector estimate for the object under consideration. We apply the PCRLB, generating a lower bound on the expected error from any estimator tracking the target [9]. Hence, the influence of the tracking algorithm is minimized. The PCRLB generates very optimistic estimates of the state vector, but allows to compare various node configurations and to identify the most promising ones in an idealized environment. The PCRLB leads to a lower bound for Σ_{xx} after one pass.

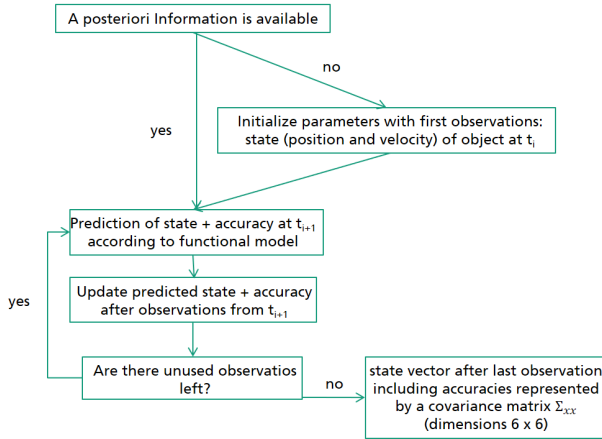


Figure 5: Tracking steps listed for each pass

During one month several passes of the same object occur, which can be combined. The state vector estimation from the prior pass can be used as prior information. If perturbation errors would be implemented, the usefulness of prior information would decrease much faster depending on orbit and radar parameters. In our case, using a priori information increases the accuracy heavily. The state of the previous pass is propagated according to a Kepler orbit till t_p , which is the first observation of the current pass. For Σ_{xx} a different approach is necessary, because the uncertainty of a Kepler orbit becomes non-Gaussian after several hours in Cartesian space [10]. That is why, a Monte Carlo Simulation is used to propagate the uncertainties. It allows to approximate arbitrary distributions [11]. With the true state and the covariance Σ_{xx} , N random samples (dimension 6 x 1) are generated. Each sample is a realization of the estimated orbit. With each realization the position and velocity of the object is calculated for t_p , such that for t_p a point cloud of N possible

states is available. Based on this cloud Σ_{pp} is approximated, which is used as a priori information for the current pass. Then the steps from Fig. 5 are repeated again. At the end of one month, the last and final state estimation of a month combines all information of all passes. Due to different orbit node geometries the time of the last pass varies for different orbits. Propagating all last covariance matrices to the same final point in time would disturb the comparison, because this would result in different propagation errors dependent on the propagation time. The covariance of the last pass is called $\Sigma_{\hat{x}\hat{x}}$ (dimension 6 x 6), which should be as small as possible for an accurate collision risk assessment. Covariance matrices can be visually represented by an error ellipsoid. Therefore, $\Sigma_{\hat{x}\hat{x}}$ can be imagined as a 6D ellipsoid. Analyzing a scalar value is easier to visualize than a 6D ellipsoid. We calculate

$$V = \sqrt{\det(\Sigma_{\hat{x}\hat{x}})}, \quad (1)$$

which is proportional to the volume of the error in the 6D state space. In the following, we call V error volume.

3.2. Error Volumes of all Setups

For each of the three setups (see Tab. 1) all of the 19 baseline configurations are tested with all 140 orbits. For each combination of baseline configuration and orbit, V (see Eq. 1) is computed after one month of observations. This results in a 140 x 19 matrix with error volumes for every configuration, which are shown in Fig. 6. The x-axis describes the length of the baseline, which corresponds to the side length of the baseline in Fig. 3. On the y-axis the error volumes, symbolized by green dots, are plotted on a \log_{10} scale. The black dots mark the median of all 140 orbits for one configuration. The black boxes describe the quartiles for the respective configuration. Evaluating which configuration is the best, one can take three different aspects into account. The easiest way is to look only at the median. If the median of a configuration is lower, one can say that this configuration is better. However, a lower median error volume does not mean that all error volumes are lower. One can take into account the black box, which represents 50 % of all V . If this box is small and the median is low, then 50 % of the simulated error volumes are low. To calculate a precise collision risk for all orbits even the highest V should be as small as possible. Thus, the third aspect is to look only at the maximum of V . Weighting these three aspects (median, quartiles, maximum) differently will lead to different conclusions. This can be identified in Fig. 6. According to the first aspect, a 600 km baseline seems the best due to the lowest median. However, the lowest quartiles are in the 250 km case. The third aspect claims that 300 km baseline is the best case. Between the maximum V in 300 km and 600 km is a difference of a factor 10^4 . The question arises if the effect of a 10^4 higher error volume is significant in terms of higher collision probability. Giving a realistic answer requires realistic error propagation of perturbations effects. The effect is also dependent on the Kepler

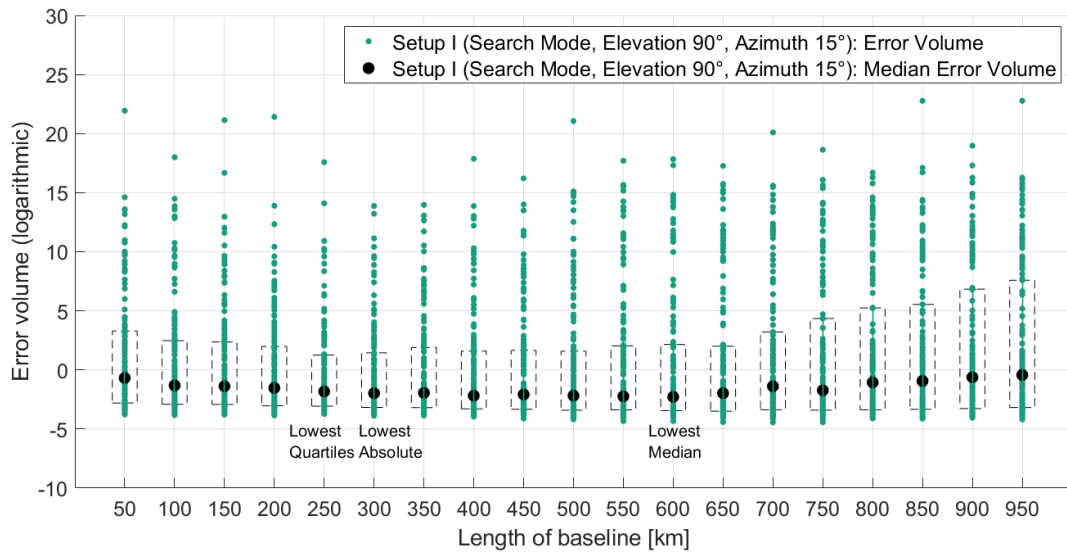


Figure 6: Setup I: FoV 90 x 15°, search mode - Effect of length of baselines on parameter estimation for all 140 tested orbits - black dots mark the median for each configuration, black boxes describe the quartiles for each configuration

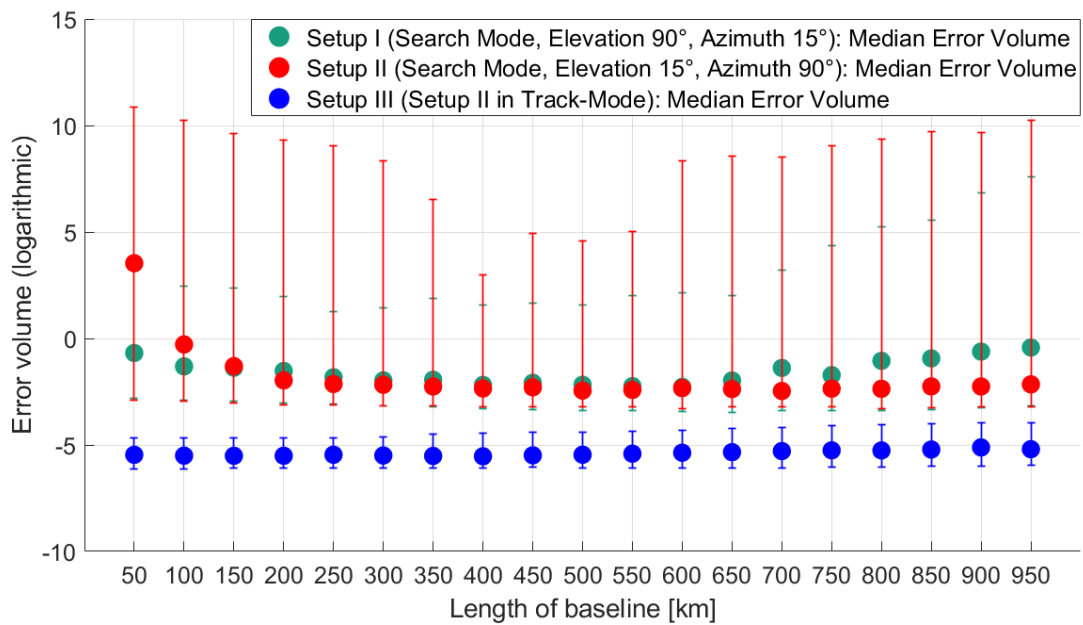


Figure 7: Median error volume for all three setups and all tested baselines (see Fig. 3) - colored dots mark the median of all 140 orbits for each configuration and each setup, error bars describe the quartiles for each configuration

parameters. These two topics should be investigated in future work.

To compare all three different setups only the median and the quartiles are shown in Fig. 7 due to aspects of clarity. The green dots mark the median of setup I, red symbolizes setup II and blue represents setup III (see Tab. 1).

Setup III has in all configurations the lowest median and the lowest quartiles. In setup III the influence of the baseline extend seems to be negligible compared to setup I and II. In setup II the median volume of all configurations is in between an interval of 10^5 . The lowest quartiles in setup II are with a 400 km baseline and in setup III with a 250 km baseline. A baseline between 200 and 600 km seems to be a good choice in all three setups. Here the medians are nearly equally low. As mentioned before, the effect of a higher error volume in terms of higher collision probability must be analyzed in further studies. For now, one can say, that in general a vertical FoV is better than a horizontal FoV, because setup I has always lower quartiles than setup II. The question arises why this is the case. One explanation is shown in Fig. 8. Here all error volumes are plotted

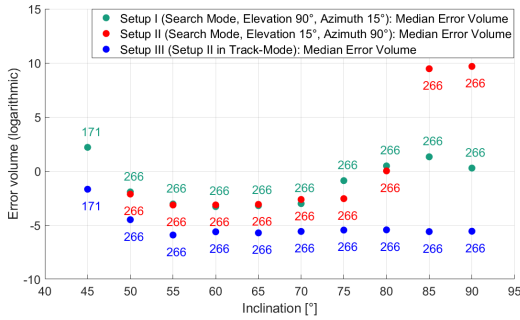


Figure 8: Error volume sorted by orbit inclination for each setup - colored dots represent median error volume, number above dot display number of observed orbits with same inclination

against the inclination of the simulated space objects and the median is visualized for all three setups. The number above the median marks the number of observed orbits with the same inclination. As it can be seen, setup I observes 171 orbits with an inclination of 45° while setup II observes none. Furthermore, at 85° and 90° inclination the medians are much lower in setup I than in setup II. Because of that, we conclude that a vertical FoV is better for orbits with a low/high inclination than a horizontal FoV. It should be mentioned that this result could change if another dwell time or search pattern is implemented.

For completeness, the error volumes are also plotted against the orbit height in Fig. 9. Again, only the median is plotted for all three setups and the number above it marks the number of observed objects. Most orbits can be observed between 600 and 1400 km orbit height. At first sight, it seems to be surprising that orbits lower than

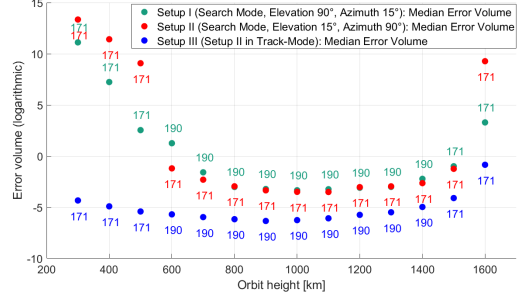


Figure 9: Error volume sorted by orbit height for each setup - colored dots represent median error volume, number above dot display number of observed orbits with same orbit height

600 km height are observed worse. Due to a shorter range to the radar a higher SNR signal is achieved and a higher accuracy should be possible. However, lower orbits lead also to shorter observation time per pass. This example highlights the importance of radar resource management. An adaptive radar dwell time or a different radar mode are beneficial for different orbit parameters, because the object can be observed longer and the higher SNR signal will deploy its full potential.

To sum it up, in all three setups a baseline between 200 and 600 km is favorable. The track mode has a higher impact on orbit estimation accuracy than the baseline between two stations. However, a track mode is not always possible since it requires prior information about an object and claims all radar resources. That is why, a search while track mode seems to be promising. We are working right now on further studies in this direction.

4. CONCLUSION

The purpose of the paper was to determine the optimal baseline between two radar nodes for orbit estimation accuracy. Hence, we varied the baseline of two radar nodes between the ranges 50 to 950 km. We simulated observations to multiple space objects and estimated their state vectors. Especially, the accuracy of the state vector using the PCRLB was analyzed. Furthermore, we implemented a search mode, a track mode, a vertical FoV and a horizontal FoV to consider their impact on the optimal baseline. This study has shown that in all setups a baseline between 200 and 600 km was favored. The second major finding was that a vertical FoV was preferred compared to a horizontal FoV in our simulations. Another result of this study indicates that the track mode has a higher impact on orbit estimation accuracy than the baseline between two stations. However, a track mode requires prior information and claims all radar resources. Since the research was limited to relative comparison between different setups, it was not possible to develop a statement in terms of collision risk analysis. The presented framework lays the groundwork for future research into radar network optimization. Beside the optimal baseline,

radar parameters, signal processing techniques or radar resource management can be optimized to minimize collision probability in space.

REFERENCES

1. T. Schildknecht, "Optical surveys for space debris," *The Astronomy and Astrophysics Review*, vol. 14, no. 1, pp. 41–111, Jan 2007. [Online]. Available: <https://doi.org/10.1007/s00159-006-0003-9>
2. M. A. Steindorfer, G. Kirchner, F. Koidl, P. Wang, and D. Kucharski, "Space debris science at the satellite laser ranging station graz," in *2017 IEEE International Conference on Environment and Electrical Engineering and 2017 IEEE Industrial and Commercial Power Systems Europe (EEEIC / I CPS Europe)*, June 2017, pp. 1–5.
3. V. S. Chernyak, *Fundamentals of multisite radar systems: multistatic radars and multistatic radar systems*. CRC Press, 1998.
4. J. Vierinen, J. Markkanen, H. Krag, J. Siminski, and A. Mancas, "Use of eiscat 3d for observations of space debris," Vierinen, JuhaMarkkanen, JussiKrag, HolgerSiminski, JanMancas, Alexandru, 2017.
5. T. Michal, J. Eglizeaud, and J. Bouchard, "Graves: The new french system for space surveillance," no. 587, 2005, pp. 61–66.
6. H. Wilden, N. ben Bekhti, R. Hoffmann, C. Kirchner, R. Kohlleppel, C. Reising, A. Brenner, and T. Eversberg, "Gestra- recent progress, mode design and signal processing," in *2019 IEEE International Symposium on Phased Array Systems and Technology*, 2019.
7. W. Niemeier, *Ausgleichsrechnung: statistische Auswertemethoden*, 2nd ed., ser. de Gruyter-Lehrbuch. Berlin u.a.: de Gruyter, 2008. [Online]. Available: <http://www.reference-global.com/isbn/978-3-11-020678-4>
8. D. A. Vallado, *Fundamentals of Astrodynamics and Applications*, 4th ed. Microcosm Press, 2013.
9. H. Van Trees and K. Bell, *Bayesian Bounds for Parameter Estimation and Nonlinear Filtering/Tracking*. Wiley, 2007. [Online]. Available: <https://books.google.de/books?id=e7hvQgAACAAJ>
10. K. T. Alfriend and I. Park, "When does uncertainty become non-gaussian," in *2016 Advanced Maui optical and Space Surveillance Technologies Conference (AMOS)*, 2067.
11. S. Thrun, B. Wolfram, and F. Dieter, *Probabilistic robotics*, ser. Intelligent robotics and autonomous agents. Cambridge, Mass. u.a.: MIT Press, 2006. [Online]. Available: <http://www.reference-global.com/doi/book/10.1515/9783110206784>